

Vanadium Extraction from Korean Vanadiferous Titanomagnetite Ore Using Alkali Roasting: Evaluation of Optimal Conditions and Leaching Rate

Youngjae kim (✉ youngjae.kim@kigam.re.kr)

Korea Institute of Geoscience and Mineral Resources

Junsoo Yoo

Korea Electronics Recycling Cooperative

Hyunsik Park

Korea Institute of Geoscience and Mineral Resources

Ho-seok Jeon

Korea Institute of Geoscience and Mineral Resources

Yosep Han

Korea Institute of Geoscience and Mineral Resources

Research Article

Keywords: vanadium, VTM, soda-roasting, water-leaching, sodium vanadate, thermodynamics

Posted Date: October 27th, 2021

DOI: <https://doi.org/10.21203/rs.3.rs-964734/v1>

License:   This work is licensed under a Creative Commons Attribution 4.0 International License.

[Read Full License](#)

Abstract

The extraction process of vanadium from vanadiferous titanomagnetite ore deposited in Korea was investigated by combining alkali roasting and water leaching processes. The effect of Na_2CO_3 addition on the efficiency with which the vanadium could be leached was investigated along with an X-ray diffraction analysis. When more than 30-wt% Na_2CO_3 was added at 1273 K, a vanadium leaching efficiency of approximately 70% was achieved. The minimum alkali-roasting temperature was determined to be 1273 K with the addition of 30-wt% Na_2CO_3 . Thermodynamic calculations revealed that the formation of the liquidus phase of Na_2CO_3 enhanced the reaction between the vanadium in the concentrate and sodium, resulting in a higher leaching efficiency for vanadium being attained. The thermodynamic calculation results were indirectly supported by the characteristic temperature determination through hot-stage microscope analysis. After 30 min of thermal treatment, a leaching efficiency for vanadium of 75% was achieved, which remained constant as the thermal treatment time was increased. Finally, the effects of the leaching time and temperature on the efficiency with which vanadium and other impurities, namely, aluminum, silicon, and sodium, could be leached was analyzed by varying the leaching time. A higher leaching efficiency was attained at higher temperatures. The leaching rate of vanadium decreased considerably after 10–20 min and subsequently remained almost constant.

1. Introduction

Ever since the discovery of vanadium in Mexican lead vanadate ore by Andrés Manuel del Rio in 1801, vanadium has been used in many fields, including the steel, aerospace, and chemical industries^{1–5}. The addition of 0.1–5.0-wt% vanadium to steel enhances the strength, hardness, and wear-resistance through grain refinement and carbide formation⁶. Approximately 85% of vanadium consumption can be attributed to the production of high-strength low-alloy steel used in high-strength pipelines for oil and gas transportation^{7,8}. In addition, vanadium is also used in tool steels, such as cutting tools and working dies. Vanadium is widely used as an alloying element for the production of titanium alloys and nickel-based superalloys. The addition of vanadium to titanium alloys and superalloys can improve both the strength of an alloy and its creep resistance at high temperatures¹. For this reason, vanadium-containing non-ferrous alloys are generally used for the construction of airframes and the blades of jet engines¹. Approximately 10% of the overall vanadium consumption can be attributed to non-ferrous aerospace alloys^{1,8}. The remaining 5% of vanadium consumption is as vanadium pentoxide catalyst for the production of sulfuric acid and maleic anhydride in the chemical industry^{8,9}. Recently, vanadium has been considered for application to energy storage systems (ESSs) because of its various redox states, which are V^{2+} , V^{3+} , V^{4+} , and V^{5+} , in an aqueous solution¹⁰. Relative to lithium-ion batteries that have caused several fires in ESS applications, vanadium redox flow batteries (VRFBs) offer cost, performance, rapid response, lifetime, and safety advantages for large-scale ESSs^{11–13}. With the increasing demand

for renewable energy, the growing interest in the use of VRFBs for ESSs seems set to lead to a rapid increase in the demand for vanadium in the energy industry.

Vanadium is the 22nd most abundant element in the Earth's crust and is more abundant than both copper and nickel ^{14,15}. However, vanadium is not observed as a concentrated mineral but is widely dispersed as a result of the replacement of the Fe³⁺ and Al³⁺ sites ^{10,16}. Vanadium is generally concentrated in magmatic titaniferous magnetite deposits or stone coal, wherein the V₂O₅ concentration is 0.2–1.0-wt% ^{17–22}. However, owing to the high extraction costs and environmental restrictions, the production of vanadium from stone coal is limited ²³. Currently, vanadiferous titanomagnetite (VTM) ore is the primary source from which vanadium is extracted.

Two major processes are used for the production of V from VTM ^{24,25}. In the first process, a VTM concentrate is introduced into an electric-arc furnace (EAF) together with anthracite, which acts as a reducing agent. During the EAF process, the magnetite in the VTM is reduced to pig iron by a carbothermic reduction. The resulting pig iron contains approximately 3.5-wt% carbon and 1.2-wt% vanadium, whereas the smelter slag contains 32-wt% TiO₂ and 0.9-wt% V₂O₅ ⁶. The vanadium present in the pig iron is removed by oxygen blowing, resulting in the formation of a vanadium-rich slag. The final products of this process are low-carbon steel and vanadium-pentoxide-concentrated slag containing 20–25-wt% V₂O₅. After cooling, crushing, and magnetic separation, the vanadium is finally recovered from the V₂O₅-rich slag as ammonium polyvanadate through the application of alkali roasting and water leaching. An example of this is the Highveld process, as used in South Africa ⁶. In the second process, the VTM is concentrated through crushing, grinding, screening, and magnetic separation, and then alkali roasted with sodium carbonate in a rotary kiln. After water leaching, the vanadium dissolved in the water is precipitated through the addition of ammonium sulfate to produce ammonium poly- or meta-vanadate with a purity > 99.5%. An example of this process is the Xstrata process used in South Africa and Australia ⁶. A common aspect of both processes ⁶ is the alkali roasting–leaching process. That is, the basic vanadium-extraction processes are similar, involving alkali roasting and water leaching. Therefore, understanding these processes is the key to successful vanadium extraction from VTM. In addition, the impurities that leach into the water in this process should be considered for application to VRFBs. The types of impurities and their concentrations in the electrolytes of VRFBs can affect the energy density, stability, and cell performance ²⁶.

In Korea, VTM ores are deposited in the Yonchon Gwan-in mine (Gyeonggi Province) ²⁷. The titanomagnetite ore bodies in Yonchon are associated with alkaline gabbroic rocks ²⁸. In the magnetite matrix, titanomagnetite is distributed as exsolution textures of thin lamellae, with vanadium concentrated in the magnetite ^{29,30}. The mineralogical characteristics, such as the associated rocks and their exsolution texture, vary with the region as a result of the differences in the original mineral formation. Therefore, the optimal conditions for vanadium extraction from Korean VTM ore would differ from the operational conditions applied to other conventional processes.

In the present study, the alkali-roasting and water-leaching processes for vanadium extraction from Korean VTM ore were studied. To achieve a high vanadium recovery efficiency, the optimal alkali roasting conditions, including temperature, time, and sodium carbonate concentration, were investigated, and thermodynamic calculations were performed. In addition, the effect of varying the temperature and time on the efficiency of the vanadium recovery in the water-leaching process was studied. The efficiencies with which other impurities, including silicon, aluminum, and sodium, could be extracted were also investigated.

2. Materials And Methods

2.1 Experimental procedure

A concentration process, including crushing, grinding, and magnetic separation, was first applied to produce a vanadium concentrate³¹. The chemical composition of the vanadium concentrate was determined by using X-ray fluorescence (XRF- 1800; Shimadzu, Kyoto, Japan). Figure 1 and Table 1 show the particle size distribution and chemical composition of the vanadium concentrate, respectively, used in this study. In this study, the D_{10} , D_{50} and D_{80} of vanadium concentrate were 11.5, 46.6, and 80.1 μm , respectively, wherein D_{10} , D_{50} and D_{80} are the specific grain sizes, which indicate that the volume proportion of particles below these particle sizes are 10%, 50%, and 90%, respectively. The vanadium concentrate was mixed with 10-, 20-, 30-, and 40-wt% Na_2CO_3 in an agate mortar to produce a homogeneous mixture. The prepared sample was then transferred to a Pt crucible (outer diameter: 45 mm, inner diameter: 44 mm, height: 42 mm) and placed in a muffle furnace at 1073, 1173, and 1273 K. During the experiment, the temperature was controlled using a proportional integral differential controller and calibrated R-type thermocouple. The sample was heated for 2 h under an air atmosphere. High-purity air was blown from 5 cm above the Pt crucible at a rate of 1000 standard cm^3/min . The oxidizing atmosphere is crucial to the alkali-roasting process for vanadium extraction because the oxidation of magnetite to hematite and the formation of the V^{5+} state could enhance the formation of sodium vanadate^{32,33}. After alkali roasting, the sample was removed from the furnace and allowed to cool to room temperature. The sample was then lightly crushed and transferred into a five-neck flask filled with distilled water. The solid-to-liquid ratio (S/L) was 1/10 (weight in gram/volume in milliliter). The five-neck flask was equipped with a temperature probe, stirrer, and condenser tube as shown in Figure 2. The sample was heated by heating mantle to 363 K while being stirred at 300 rpm for 4 h. For the leaching kinetic study, approximately 5 mL of the sample solution was collected using a syringe equipped with a syringe filter (pore size 0.2 μm) at different times. To verify the reproducibility, the water-leaching experiment was repeated three times at different temperatures. After water leaching, the solution was filtered using a vacuum bottle-top filter (with a pore size of 0.22 μm). The chemical composition and its concentration in the water were analyzed using inductively coupled plasma–optical emission spectroscopy (ICP-OES, 5300DV, Perkin Elmer, NY, USA). To determine the chemical composition of the filtered residual, alkali fusion was conducted according to the test method used for soil³⁴. Approximately 0.1 g of residual was weighed and mixed with 1 g of lithium tetraborate. The mixture was then transferred

to a carbon crucible and melted at 1273 K under an argon atmosphere. After 1 h, the sample was quenched to produce a non-crystalline sample. The obtained glassy sample was ground and sieved through a 100 μm mesh. The powder sample was transferred to a 200 mL beaker and completely leached using aqua regia at 493 K on a heating plate. Subsequently, the chemical composition and concentration in the leachate solution were analyzed using ICP-OES. Finally, the leaching efficiency for component A was determined using (1).

Table 1
Chemical composition of vanadium concentrate (wt%).

SiO ₂	Al ₂ O ₃	Fe ₃ O ₄	CaO	MgO	K ₂ O	TiO ₂	MnO	V ₂ O ₅
5.49	3.94	67.32	0.91	3.52	0.13	17.54	0.34	0.79

$$\frac{(\text{Concentration of A in water})}{(\text{Concentration of A in water}) + (\text{Concentration of A in residual})} \times 100$$

1

2.2 Characterization

The crystalline phases of the VTM concentrate before and after thermal treatment were determined by X-ray diffraction (XRD; D/Max 2200; Rigaku, Tokyo, Japan). At a scanning rate of 4°/min, the diffraction pattern was collected within a 2θ range of 10°–90°. During the analysis, the power was maintained at 40 kV and 30 mA, with X-rays being generated using a copper tube.

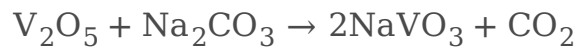
The sintering, softening, and melting temperatures were determined using a hot-stage microscope (HSM; Misura, Expert System, Modena, Italy). A cylinder-type test sample with a diameter of 2 mm and height of 3 mm was prepared by uniaxial pressing. The sample was placed on an alumina plate and then loaded into the HSM. During the experiment, the temperature was rapidly increased at a rate of 20 K/min from room temperature to 673 K. The temperature was then slowly increased at a rate of 10 K/min, and the shape change was recorded via a microscope equipped for image processing. With the aid of the image-processing software supplied with the instrument, the changes in the sample height and height/width ratio as the temperature was varied were calculated. By applying the standard test method, the characteristic temperatures (sintering, softening, and melting temperatures) were determined. A more detailed procedure and measurement principle appears in the literature^{35,36}.

3. Results And Discussion

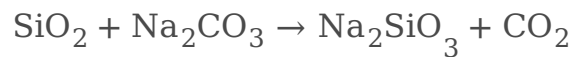
3.1 Effect of Na₂CO₃ addition on leaching efficiency in alkali-roasting process

Figure 3 shows the effect of Na₂CO₃ addition on the leaching efficiencies for vanadium, sodium, silicon, and aluminum. The leaching efficiencies for titanium and iron were also analyzed, but the results were less than 0.05%. According to a previous study, the dissolution of Ti and Fe is thermodynamically unfavorable after alkali roasting¹⁰. Therefore, the leaching efficiencies for titanium and iron were not considered in the present study. The leaching efficiency for vanadium increases considerably from 27.9–64.0% when the Na₂CO₃ concentration is increased from 10- to 20-wt%. Subsequently, the leaching efficiency for vanadium gradually increases with the addition of Na₂CO₃. A similar relationship is observed for sodium, silicon, and aluminum. With the addition of 20- or 30-wt% Na₂CO₃, the efficiency with which aluminum, silicon, and sodium could be leached increases considerably.

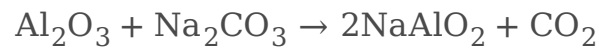
According to the thermochemical modeling study¹⁰, the oxides in the vanadium concentrate are converted into water-soluble sodium compounds during the alkali roasting.



2



3

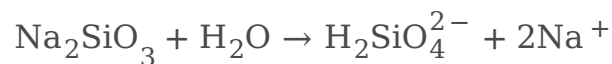


4

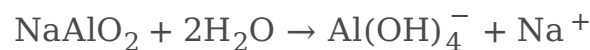
The dissolution of sodium compounds in water, as defined by (2), (3), and (4), is thermodynamically favorable¹⁰.



5



6



7

Therefore, the increase in the leaching efficiency with the concentration of Na₂CO₃ is directly related to the formation of sodium compounds. Figure 4 shows the XRD pattern for the vanadium concentrate and the XRD results after alkali roasting at 1273 K with different concentrations of Na₂CO₃. The vanadium concentrate of Korean VTM consists mainly of magnesioferrite ((Mg²⁺, Fe²⁺)₃O₄) and ilmenite (FeTiO₃).

Once the vanadium concentrate is oxidized with 10-wt% Na_2CO_3 at 1273 K, the ferrous (Fe^{2+}) state in the vanadium concentrate converts into a ferric state (Fe^{3+}) to form a hematite (Fe_2O_3) phase. Sodium is not observed when 10-wt% Na_2CO_3 is added. This result implies that the 10-wt% Na_2CO_3 is insufficient to form enough sodium compounds during the heat treatment. As a result, low leaching efficiencies for vanadium, silicon, and aluminum are observed, as shown in Fig. 3. As the Na_2CO_3 addition is increased from 10 to 20-wt%, the formation of the sodium iron titanium oxide (NaFeTiO_4) phase is observed along with the hematite phase. Above 30-wt% Na_2CO_3 , the crystalline peak of the hematite phase disappears, and the formation of sodium iron oxide silicate ($\text{NaFeO}_{2.35}\text{Si}_{0.175}$) and another sodium iron titanium oxide ($\text{Na}_{0.75}\text{Fe}_{0.75}\text{Ti}_{0.25}\text{O}_2$) phase is observed. As the Na_2CO_3 concentration is increased from 20- to 40-wt%, the intensity of the sodium compound peaks gradually increases, implying a quantitative increase in the related phases. The XRD results do not feature a vanadium-related crystalline phase because of the low concentration of the vanadium concentrate. However, it can be inferred that the formation of the sodium vanadate phase increases with the amount of iron-bearing sodium compounds, given that vanadium exists in the VTM replacing the Fe^{3+} sites. For this reason, the leaching efficiency for vanadium gradually increased with the addition of 20-wt% Na_2CO_3 .

3.2 Effect of thermal treatment temperature on leaching efficiency in alkali-roasting process

Figure 5 shows the effect of the thermal treatment temperature and time on the leaching efficiencies for vanadium, sodium, silicon, and aluminum. The leaching efficiencies for vanadium and sodium are initially maintained as the temperature increases from 1073 to 1173 K. However, the leaching efficiency for vanadium increases greatly as the temperature increases to 1273 K. On the other hand, the leaching efficiency for sodium decreases as the temperature increases to 1273 K. The leaching efficiency for silicon is not significantly affected by the temperature change. However, the leaching efficiency for aluminum increases monotonously with the temperature. The effect of the thermal treatment time on the leaching efficiency is not significant. The leaching efficiency for vanadium remains almost constant at approximately 75% after 30 min of thermal treatment. It seems that a thermal treatment time of 30 min is sufficient to form the water-soluble sodium vanadate needed to recover the vanadium from the vanadium concentrate during the alkali-roasting process.

To investigate the effect of temperature on the leaching efficiency for vanadium, thermodynamically stable phases were calculated at different temperatures using the FactSage 8.0 thermochemical software (Thermfact and GTT-Technologies, Montreal, Canada). Figure 6 shows the thermodynamically stable phases at temperatures between 1023 and 1473 K when the vanadium concentrate was mixed with 30-wt% Na_2CO_3 under the oxidizing atmosphere. The liquid sodium vanadate (NaVO_3) phase can be observed over a wide temperature range from 1023 to 1423 K, inferring that the alkali-roasting process can be performed even at 1023 K. However, this thermodynamic calculation is carried out assuming that all the components in the vanadium concentrate can equally come in contact and react with the Na_2CO_3 for a sufficiently long time. Considering the complicated micromorphology of the Korean VTM mineral ²⁹,

as well as the limited reaction time, the formation of the liquidus sodium vanadate phase through the reaction of the vanadium concentrate with solid Na_2CO_3 would be difficult practically. The liquidus Na_2CO_3 phase is formed at 1273 K, in which the leaching efficiency for vanadium increases considerably, inferring that the formation of the liquidus sodium carbonate phase promotes the reaction between the Na_2CO_3 and vanadium by penetrating the microstructure in the VTM. The formation of a molten Na_2CO_3 phase is indirectly supported by the HSM analysis results. As shown in Fig. 7, the softening temperature of the system containing 30-wt% Na_2CO_3 is in good agreement with the temperature at which the molten Na_2CO_3 phase is observed in the thermodynamic calculations. On the other hand, the melting temperature of the system containing 30-wt% Na_2CO_3 is in excellent agreement with the solidus temperature, wherein the molten slag phase is first observed by thermodynamic calculations. Given that the alkali-roasting process is performed in a rotary furnace, the formation of the molten slag phase would be detrimental to the operation due to the low fluidity and reaction between the refractory and molten slag. Therefore, alkali roasting above 1373 K is not recommended for Korean VTM when the vanadium concentrate is mixed with 30-wt% Na_2CO_3 .

3.3 Effect of leaching temperature and time on leaching efficiency in water-leaching process

In the aqueous state, vanadium has various redox states that range from 2 to 5, depending on the pH. Figure 8 shows the Pourbaix diagrams for a 0.01 mol/L vanadium solution at 298 and 363 K, as calculated by FactSage 8.0. The pentavalent vanadium is stable over a wide range of pH values. The stable species of vanadium does not change significantly as the temperature increases. In the present study, the pH and oxidation-reduction potential (ORP) reach approximately 13 and 380 mV, respectively, over a leaching time of 1 min, whereas the pH and ORP remain almost constant over a leaching time of 4 h. It can be inferred that the stable ionic state of vanadium does not change significantly with the leaching times and temperatures. According to the calculated E-pH diagram shown in Fig. 8, the stable vanadium species is VO_4^- in the water-leaching solution.

Figure 9 shows the leaching efficiency for vanadium for different leaching times and temperatures. Prior to the water leaching, alkali roasting was conducted at 1273 K for 2 h in a mixture with 30-wt% Na_2CO_3 . A higher leaching efficiency for vanadium can be observed as the leaching temperature increases. The leaching efficiency for vanadium increases considerably during the initial stage. Subsequently, the rate of increase slows but then gradually increases after 10–20 min. This change in the leaching rate has been explained in an earlier study of vanadium leaching kinetics using sulfuric acid by the shrinking-core model³⁷. In their study, rapid vanadium extraction was observed within 0–10 min. The leaching rate slowed after 10 min and remained constant after 50 min. Similar results have been reported for other studies addressing vanadium extraction using sulfuric acid³⁸. These studies revealed that the rate-determining step changes as the leaching process progresses. Therefore, in the present study, the drastic decrease in the leaching rate implies that the vanadium extraction is controlled by a rate-determining step (such as transportation, solid diffusion, or surface reaction) after 10–20 min of leaching.

The leaching efficiencies for other impurities such as aluminum, silicon, and sodium were also investigated. The results are shown in Fig. 10. Prior to the water leaching, alkali roasting was conducted at 1273 K for 2 h in a mixture of 30-wt% Na₂CO₃. The higher leaching temperature results in a higher leaching efficiency for both aluminum and sodium. However, the leaching efficiency for silicon initially increases with the temperature from 298 to 333 K but decreases above 363 K. Similar to the change in the leaching rate for vanadium, the leaching efficiency for the impurities increases considerably in the initial stage. However, after 10–30 min, the leaching rate slows first but then gradually increases with the leaching time. Considering the precipitation process followed for vanadium extraction, the impurity elements should be restricted to a certain concentration in the vanadium-rich solution³⁹. The results obtained for the leaching efficiency for vanadium and impurities in the present study would be useful for determining the leaching time and temperature for the leaching process.

4. Conclusions

To develop a vanadium extraction process utilizing VTM ore deposited in Korea, the conditions under which alkali roasting and water leaching are performed were investigated. An increase in the leaching efficiency for vanadium was observed as the amount of Na₂CO₃ was increased. Once the amount of Na₂CO₃ exceeded 20-wt%, the hematite phase gradually disappeared, and the intensity of the sodium-containing phases increased. It appears that at least 30-wt% Na₂CO₃ was required to instigate a sufficient reaction between VTM and sodium carbonate at 1273 K. The effects of the temperature and thermal treatment time on the leaching efficiency for vanadium and other impurities, including silicon, aluminum, and sodium, were analyzed. The leaching efficiency for vanadium was maintained as the temperature increased from 1073 to 1173 K, but greatly increased above 1273 K when the Na₂CO₃ concentration was 30-wt%. The thermodynamic calculation results pointed to the formation of the liquidus Na₂CO₃ phase at 1273 K. The softening temperature observed with the hot-stage microscope was in excellent agreement with the temperature at which the molten Na₂CO₃ phase formed. The molten Na₂CO₃ phase could penetrate the complicated microstructure in VTM ore and enhances the probability of there being a reaction between the sodium and vanadium. A thermodynamic study showed that alkali roasting above 1373 K could not be recommended because of the formation of the molten slag phase. A thermal treatment time of 30 min appears to be sufficient when the alkali-roasting process is carried out with 30-wt% Na₂CO₃ at 1273 K. The leaching efficiency reached 75% and remained constant. Finally, the effects of the leaching time and temperature on the leaching efficiency were investigated. The results of thermodynamic calculations indicated that the stable species of vanadium in the water-leaching process was VO₄⁻ under the present experimental conditions. Higher leaching efficiencies for vanadium and other impurities were observed as the leaching temperature was increased. The leaching efficiency for vanadium increased greatly in the initial stage and remained almost constant after 10–20 min of leaching time. However, the change in the leaching rate varied depending on the impurities that were present. Understanding the leaching efficiency for vanadium and other impurities would be useful for optimizing the conditions for the water-leaching process, considering the vanadium precipitation process.

Declarations

Acknowledgements

The authors are grateful for the financial support provided by the Basic Research Project (GP2020-013) of the Korea Institute of Geoscience and Mineral Resources (KIGAM), funded by the Ministry of Science and ICT.

Conflicts of interest

The authors declare no conflicts of interest.

References

1. Bauer, G. *et al.* Vanadium and Vanadium Compounds. in *Ullmann's Encyclopedia of Industrial Chemistry* 1–22 (Wiley-VCH Verlag GmbH & Co. KGaA, 2017). doi:10.1002/14356007.a27_367.pub2.
2. Taylor, P. R., Shuey, S. A., Vidal, E. E. & Gomez, J. C. Extractive metallurgy of vanadium-containing titaniferous magnetite ores: A review. *Miner. Metall. Process.* **23**, 80–86 (2006).
3. Kelley, K. D., Scott, C., Polyak, D. E. & Kimball, B. E. *Vanadium*. (2017) doi:10.3133/pp1802U.
4. Lee, J. *et al.* A review on the metallurgical recycling of vanadium from slags: towards a sustainable vanadium production. *J. Mater. Res. Technol.* **184**, 107229 (2021).
5. Zhang, C., Sun, C., Li, H., Yin, W. & Zhou, J. Blank roasting kinetics of illite type vanadium bearing stone coal. *J. Mater. Res. Technol.* **9**, 7363–7369 (2020).
6. Cardarelli, F. *Materials Handbook - A Concise Desktop Reference*. (Springer International Publishing, 2018). doi:10.1007/978-3-319-38925-7.
7. Rohrmann, B. Vanadium in South Africa. *J. South. African Inst. Min. Metall.* **85**, 141–150 (1985).
8. Swinbourne, D. R., Richardson, T. & Cabaltega, F. Understanding ferrovanadium smelting through computational thermodynamics modelling. *Trans. Institutions Min. Metall. Sect. C Miner. Process. Extr. Metall.* **125**, 45–55 (2016).
9. Langeslay, R. R. *et al.* Catalytic Applications of Vanadium: A Mechanistic Perspective. *Chem. Rev.* **119**, 2128–2191 (2019).
10. Gilligan, R. & Nikoloski, A. N. The extraction of vanadium from titanomagnetites and other sources. *Miner. Eng.* **146**, 106106 (2020).
11. Leung, P. *et al.* Progress in redox flow batteries, remaining challenges and their applications in energy storage. *RSC Adv.* **2**, 10125 (2012).
12. Lee, D. *et al.* Aminopropyl Functionalized Silica Nanoparticle Dispersed Nafion Composite Membranes for Vanadium Redox Flow Batteries. *Membr. J.* **30**, 307–318 (2020).
13. Doetsch, C. & Pohlig, A. The Use of Flow Batteries in Storing Electricity for National Grids. in *Future Energy - Improved, Sustainable and Clean Options for our Planet* (ed. Letcher, T. M.) 263–277

(Elsevier, 2020). doi:10.1016/B978-0-08-102886-5.00013-X.

14. Zhang, G. *et al.* Simultaneous extraction of vanadium and titanium from vanadium slag using ammonium sulfate roasting-leaching process. *J. Alloys Compd.* **742**, 504–511 (2018).
15. Zhang, Y. M., Bao, S. X., Liu, T., Chen, T. J. & Huang, J. The technology of extracting vanadium from stone coal in China: History, current status and future prospects. *Hydrometallurgy* **109**, 116–124 (2011).
16. Hu, P. *et al.* Highly selective separation of vanadium over iron from stone coal by oxalic acid leaching. *J. Ind. Eng. Chem.* **45**, 241–247 (2017).
17. Fischer, R. P. *Vanadium resources in titaniferous magnetite deposits.* (1975) doi:10.3133/pp926B.
18. Cai, Z., Feng, Y., Li, H., Du, Z. & Liu, X. Hydrometallurgy Co-recovery of manganese from low-grade pyrolusite and vanadium from stone coal using fluidized roasting coupling technology. *Hydrometallurgy* **131–132**, 40–45 (2013).
19. Zheng, Q., Zhang, Y., Liu, T., Huang, J. & Xue, N. Hydrometallurgy Vanadium extraction from black shale: Enhanced leaching due to fluoride addition. *Hydrometallurgy* **187**, 141–148 (2019).
20. Hukkanen, E. & Walden, H. The production of vanadium and steel from titanomagnetites. *Int. J. Miner. Process.* **15**, 89–102 (1985).
21. Zhang, Y. *et al.* A novel process for the recovery of iron, titanium, and vanadium from vanadium-bearing titanomagnetite: sodium modification–direct reduction coupled process. *Int. J. Miner. Metall. Mater.* **24**, 504–511 (2017).
22. Ghoddy Nejad, D., Taghizadeh, M. & Khanchi, A. Vanadium extraction from a magnetite ore using alkaline roasting and acid leaching processes: optimization of parameters by response surface methodology. *J. Min. Environ.* **10**, 241–255 (2019).
23. BUSHVELD Minerals. Vanadium Market Overview. in *Bushveld Minerals Annual Report and Financial Results* 21–25 (BUSHVELD Minerals, 2019).
24. Jena, B. C. C., Dresler, W. & Reilly, I. G. G. Extraction of titanium, vanadium and iron from titanomagnetite deposits at Pipestone Lake, Manitoba, Canada. *Miner. Eng.* **8**, 159–168 (1995).
25. Habashi, F. *Handbook of extractive metallurgy.* (Wiley-VCH, 1997).
26. Cao, L., Skyllas-Kazacos, M., Menictas, C. & Noack, J. A review of electrolyte additives and impurities in vanadium redox flow batteries. *J. Energy Chem.* **27**, 1269–1291 (2018).
27. Han, Y. *et al.* Magnetic Separation Behavior of V, Ti, and Fe of Fractured Products from Domestic Vanadium Titanium-Magnetite (VTM) Ore. *J. Korean Soc. Miner. Energy Resour. Eng.* **58**, 10–16 (2021).
28. Kim, K. H., Lee, H. J. & Chon, H. T. Ore Genesis of the Yonchon Titaniferous Iron. Ore Deposits, South Korea. *Econ. Environ. Geol.* **27**, 117–130 (1994).
29. Lee, S. A Review on Types of Vanadium Deposits and Process Mineralogical Characteristics. *J. Korean Soc. Miner. Energy Resour. Eng.* **57**, 640–651 (2020).

30. Kim, S.-M. & Jeon, H.-S. Separation Processes for Self-Sufficient Recovery of Vanadium Resources in Korea. *J. Korean Soc. Miner. Energy Resour. Eng.* **56**, 292–302 (2019).
31. Go, B. *et al.* Development of Separation Technique for the Production of Vanadium from Domestic Vanadium Titanomagnetite Ore. *J. Korean Soc. Miner. Energy Resour. Eng.* **58**, 2–9 (2021).
32. Lam, S. W. & Harris, D. Vanadium. in *SME Mineral Processing and Extractive Metallurgy Handbook* (eds. Kawatra, S. K. & Young, C. A.) 2185–2196 (SOCIETY FOR MINING, METALLURGY & EXPLORATION, 2019).
33. Peng, H. A literature review on leaching and recovery of vanadium. *J. Environ. Chem. Eng.* **7**, 103313 (2019).
34. Pansu, M. & Gautheyrou, J. Analysis of Extractable and Total Elements. in *Handbook of Soil Analysis* 895–974 (Springer Berlin Heidelberg, 2006). doi:10.1007/978-3-540-31211-6.
35. Salem, S., Jazayeri, S. H., Bondioli, F., Allahverdi, A. & Shirvani, M. Characterizing thermal behavior of ceramic glaze containing nano-sized cobalt-aluminate pigment by hot stage microscopy. *Thermochim. Acta* **521**, 191–196 (2011).
36. Panna, W., Wyszomirski, P. & Kohut, P. Application of hot-stage microscopy to evaluating sample morphology changes on heating. *J. Therm. Anal. Calorim.* **125**, 1053–1059 (2016).
37. Yang, Z. *et al.* Leaching kinetics of calcification roasted vanadium slag with high CaO content by sulfuric acid. *Int. J. Miner. Process.* **133**, 105–111 (2014).
38. Aarabi-Karasgani, M., Rashchi, F., Mostoufi, N. & Vahidi, E. Leaching of vanadium from LD converter slag using sulfuric acid. *Hydrometallurgy* **102**, 14–21 (2010).
39. Zhu, X., Li, W., Tang, S. & Li, W. Effect of Impurity Ions on Vanadium Precipitation in Vanadium-rich Solution. *J. Min. World Express* **5**, 28 (2016).

Figures

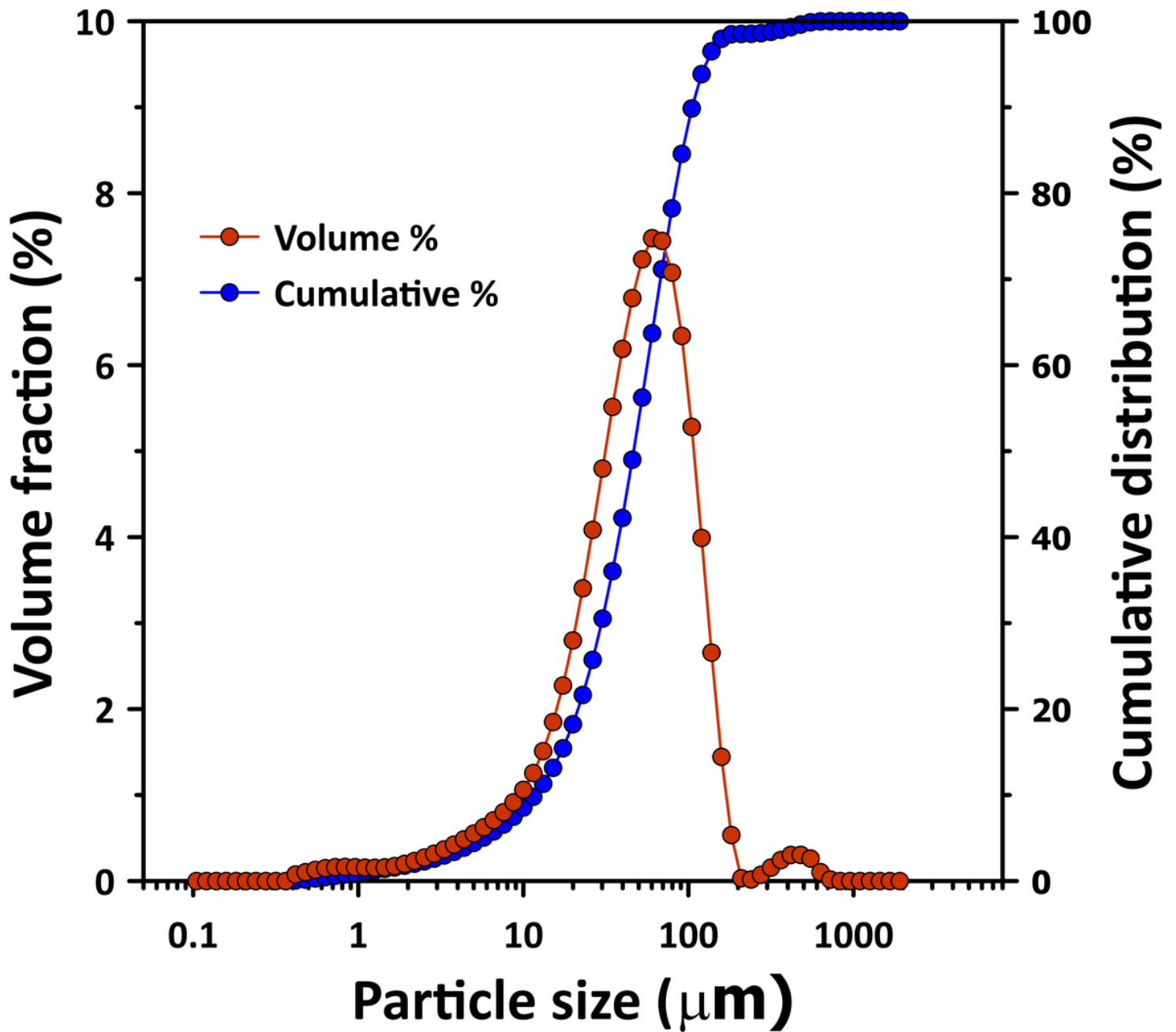


Figure 1

Particle size distributions of the vanadium concentrate prepared from milled vanadiferous titanomagnetite (VTM) samples: volume fraction percentage (red circle line) and cumulative distribution percentage (blue circle line).

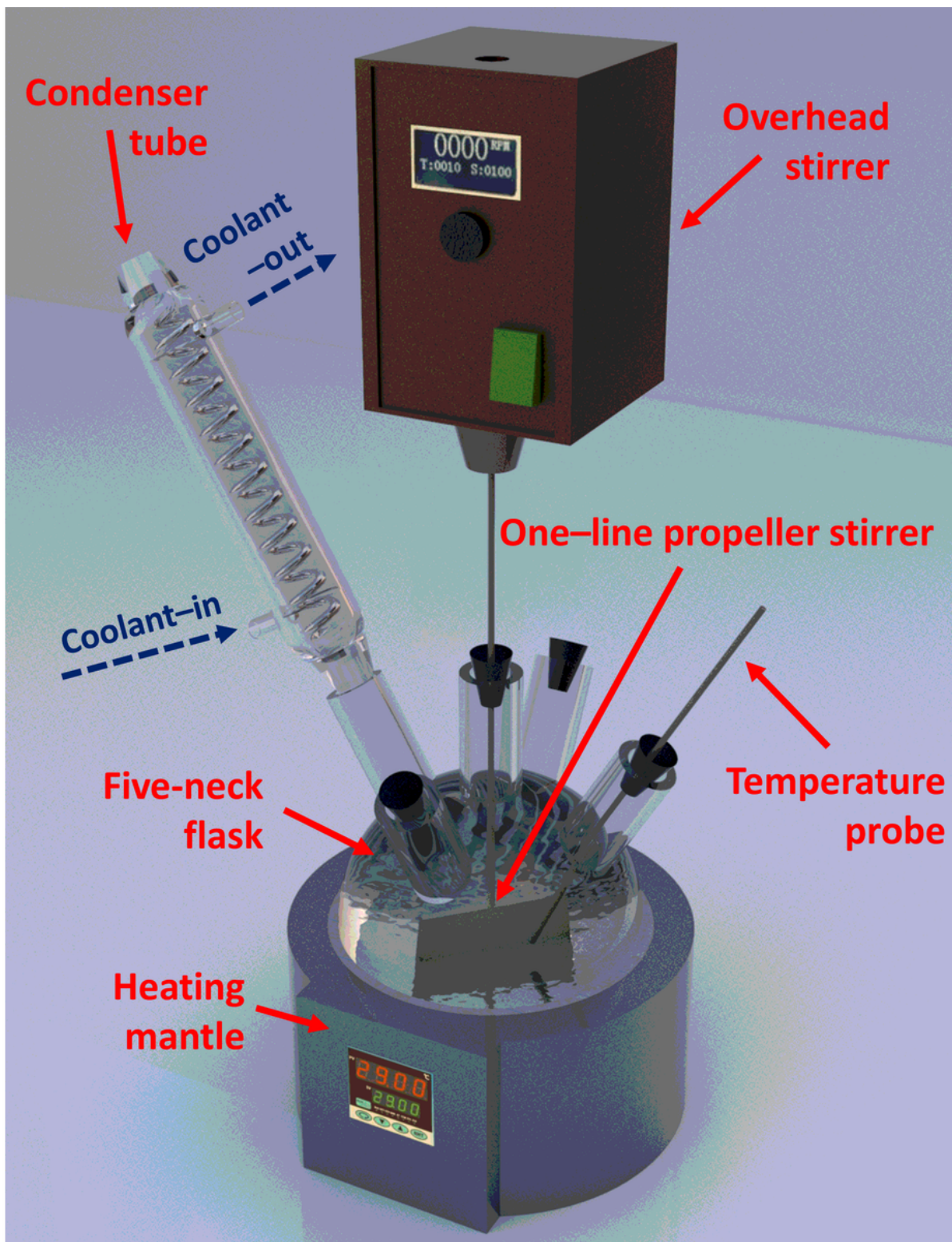


Figure 2

Schematic of apparatus used in water-leaching experiment.

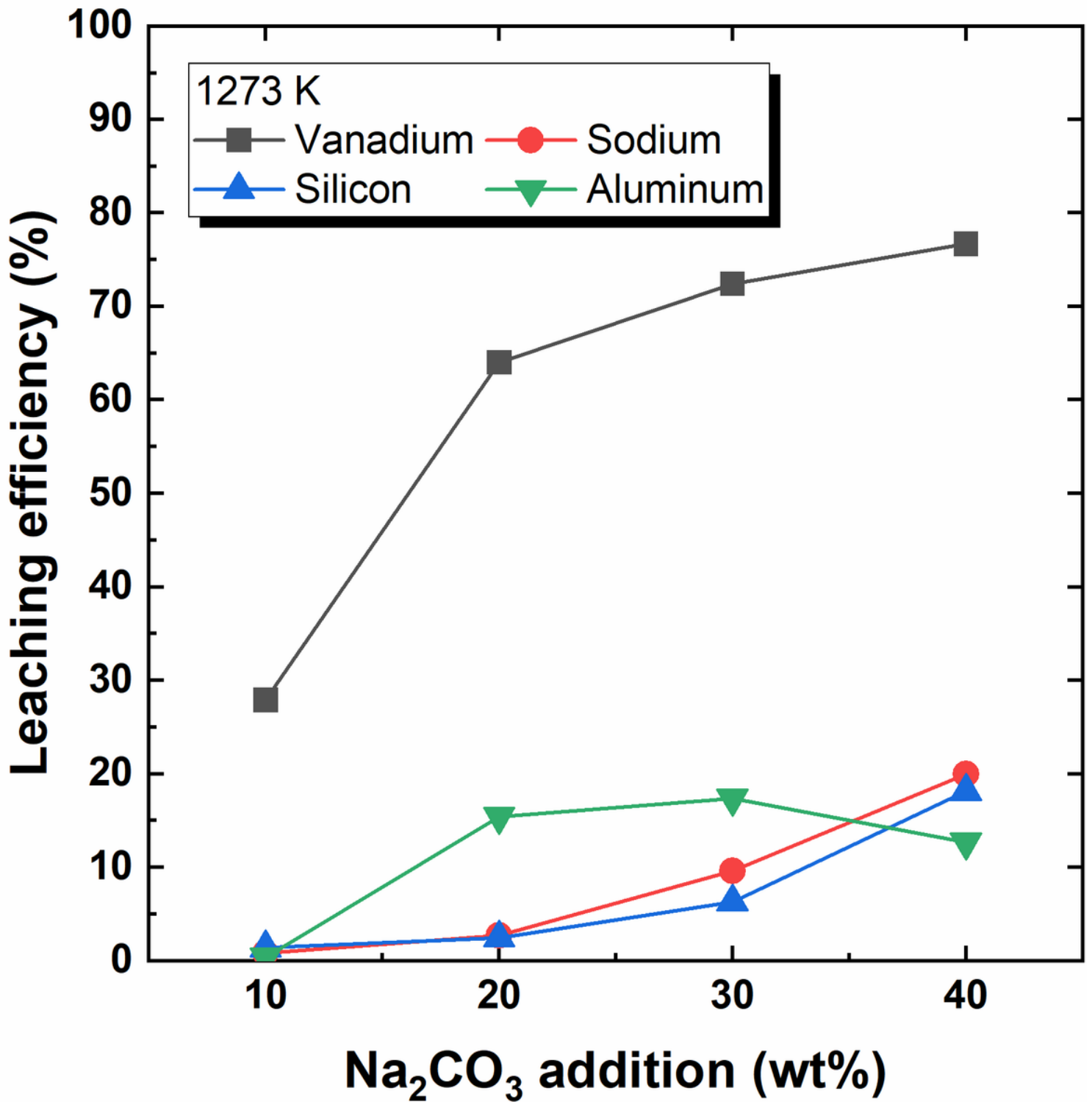


Figure 3

Effect of Na₂CO₃ addition on leaching efficiency for vanadium, sodium, silicon, and aluminum in the alkali-roasting process.

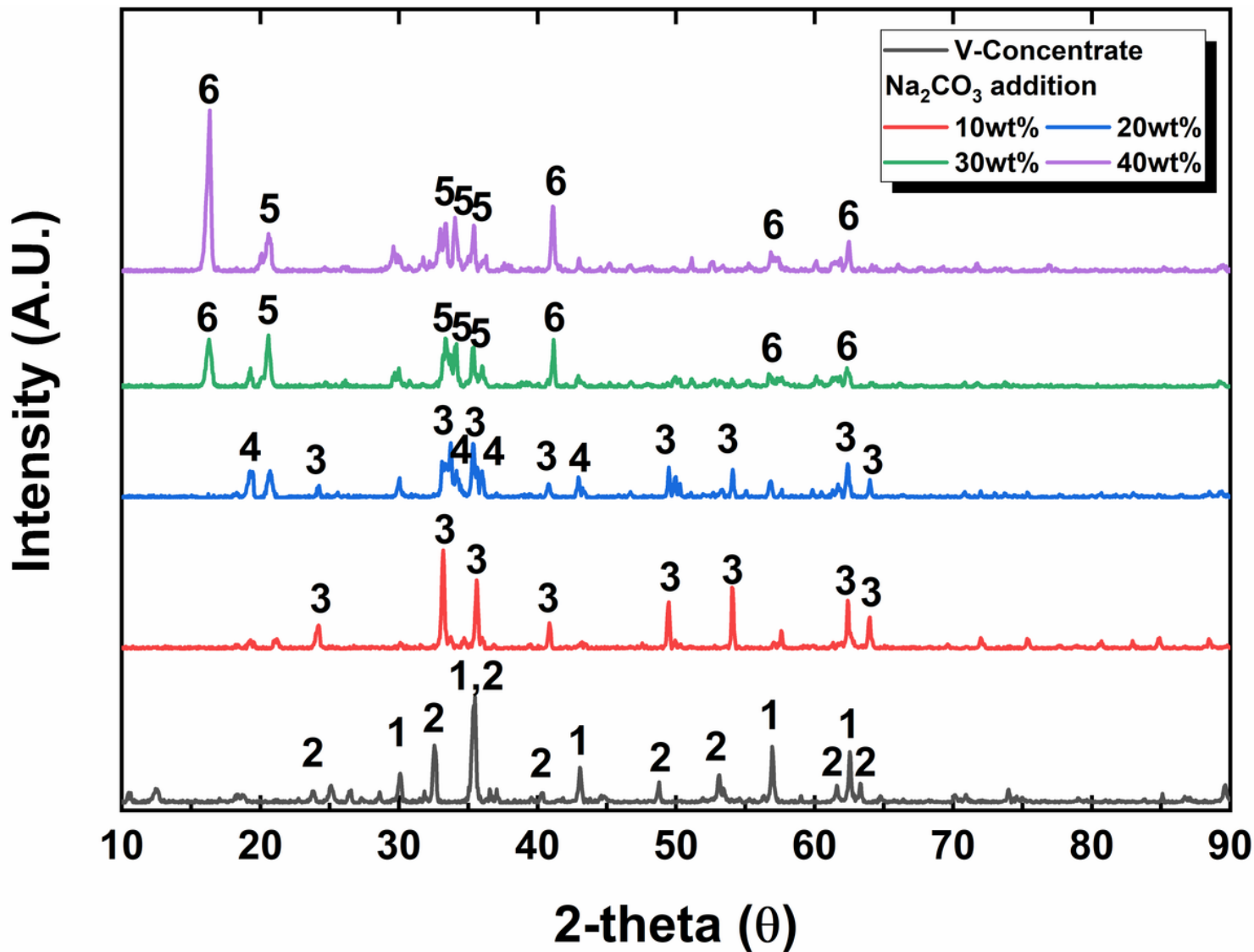


Figure 4

X-ray diffraction patterns of thermally treated vanadium concentrate with a range of Na₂CO₃ concentrations. (1: Magnesioferrite ((Mg²⁺, Fe²⁺)₃O₄), 2: Ilmenite (FeTiO₃), 3: Hematite (Fe₂O₃), 4: Sodium iron titanium oxide (NaFeTiO₄), 5: Sodium iron oxide silicate (NaFeO_{2.35}Si_{0.175}), and 6: Sodium iron titanium oxide₂ (Na_{0.75}Fe_{0.75}Ti_{0.25}O₂))

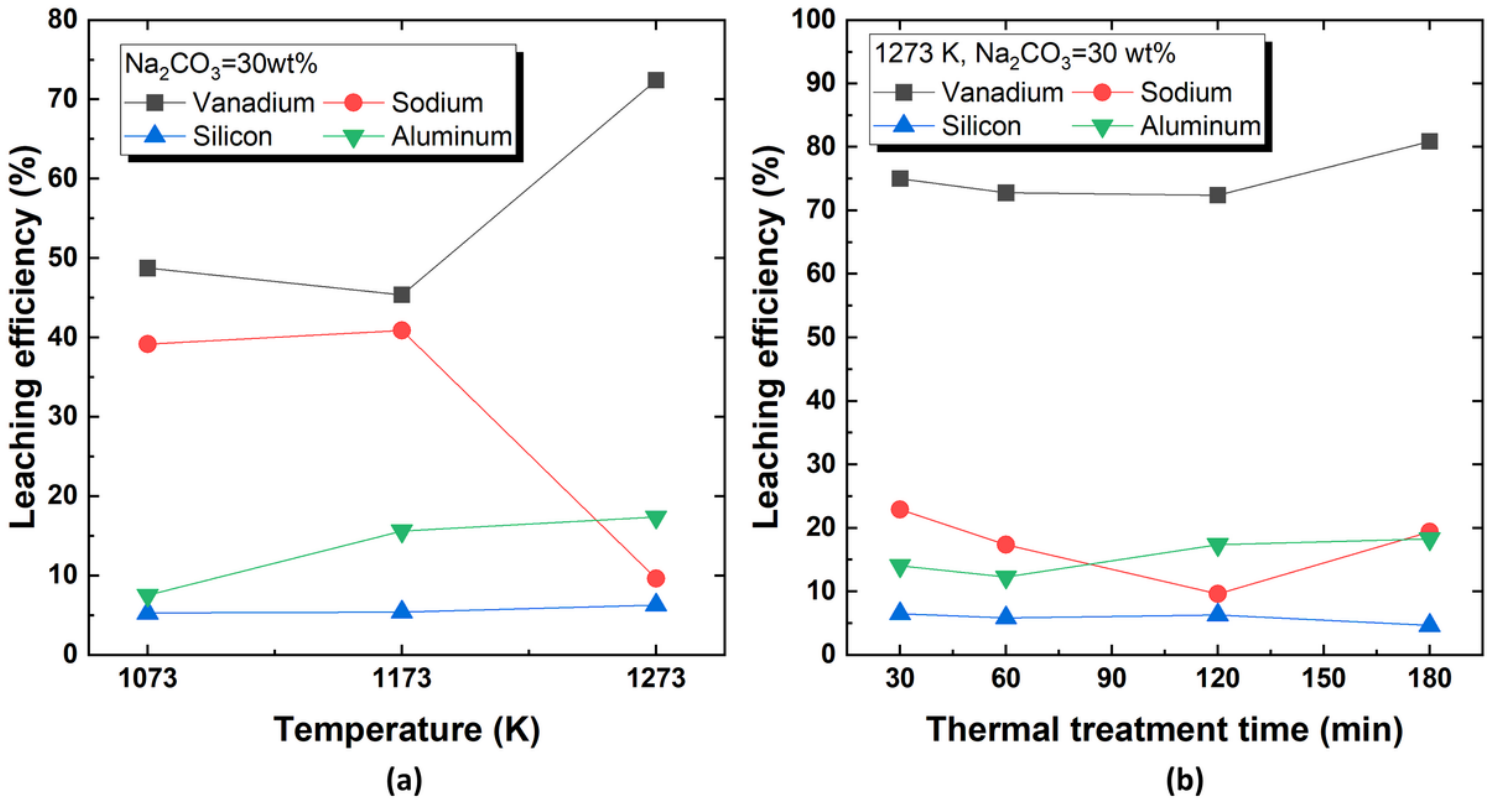


Figure 5

Effect of (a) temperature and (b) thermal treatment time on the leaching efficiency for vanadium, sodium, silicon, and aluminum in the alkali-roasting process.

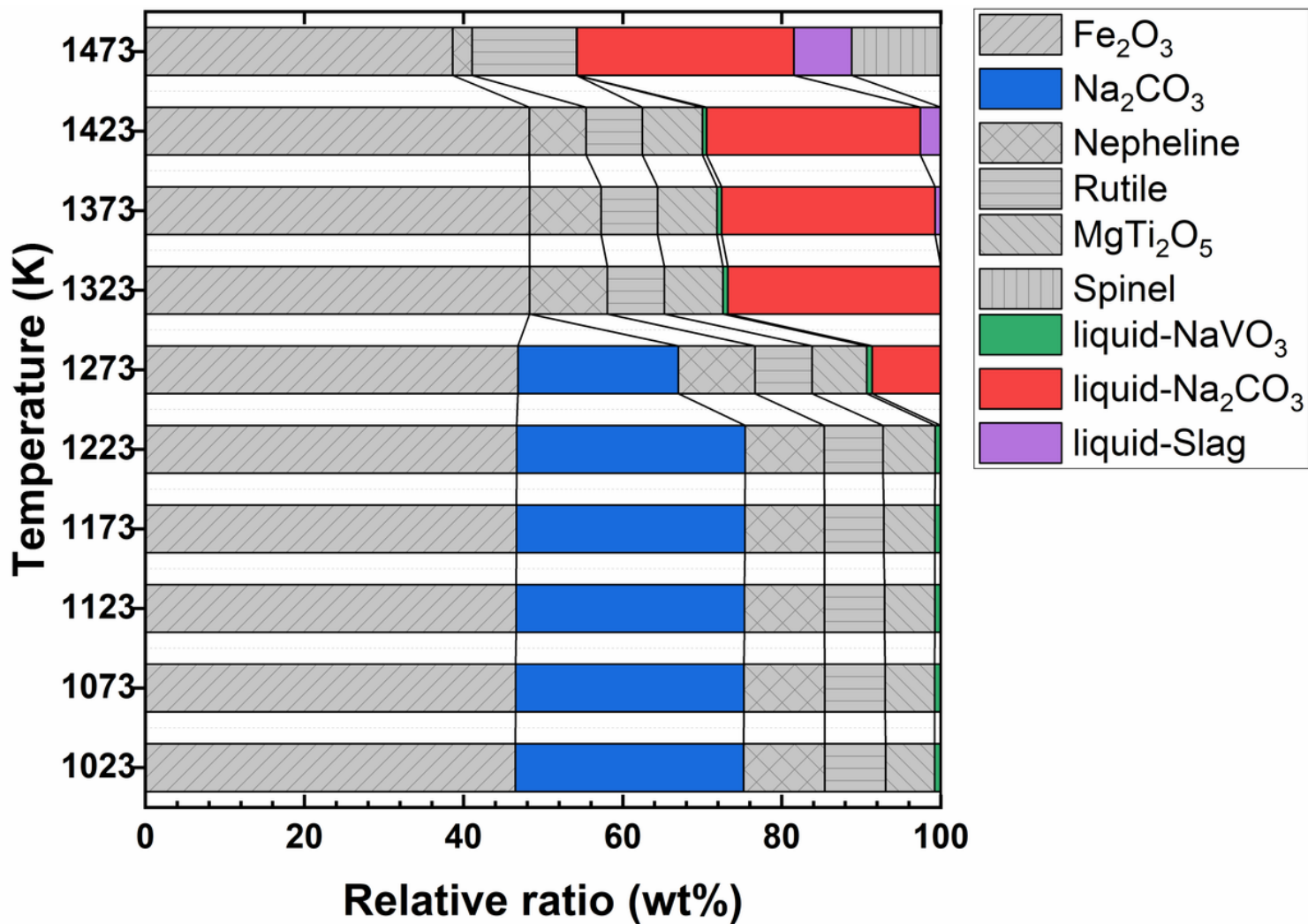


Figure 6

Relative ratio (wt%) of thermodynamic equilibrium phases calculated for the mixture of vanadium concentrate and 30-wt% Na₂CO₃ at different temperatures.

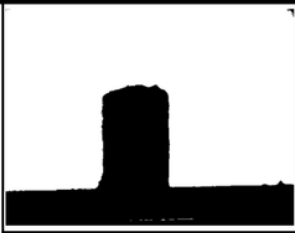
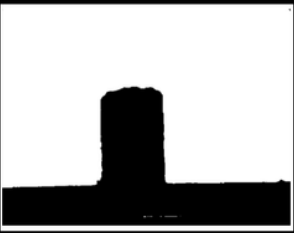
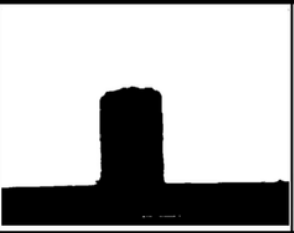
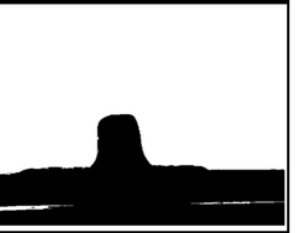



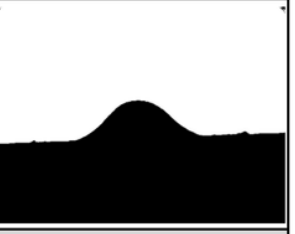
Na ₂ CO ₃ addition	Initial	Sintering temperature	Softening temperature	Melting temperature
10 wt%	 673 K	 1408 K	 1410 K	 1897 K
30 wt%	 673 K	 1286 K	 1288 K	 1396 K

Figure 7

Characteristic temperatures (K) of the vanadium concentrate mixed with 10- and 30-wt% Na₂CO₃, as determined using hot-stage microscope.

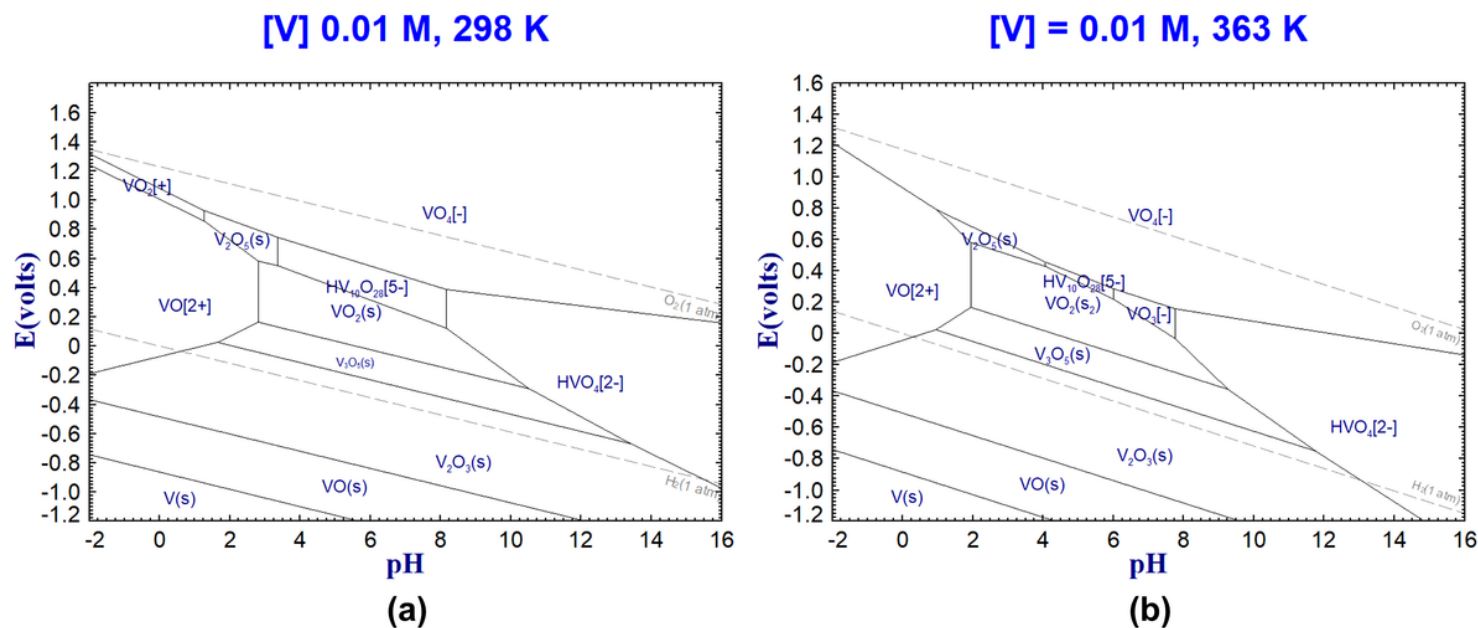


Figure 8

Calculated E-pH diagram showing distribution of vanadium species in 0.01 mol/L vanadium solution at (a) 298 K and (b) 363 K.

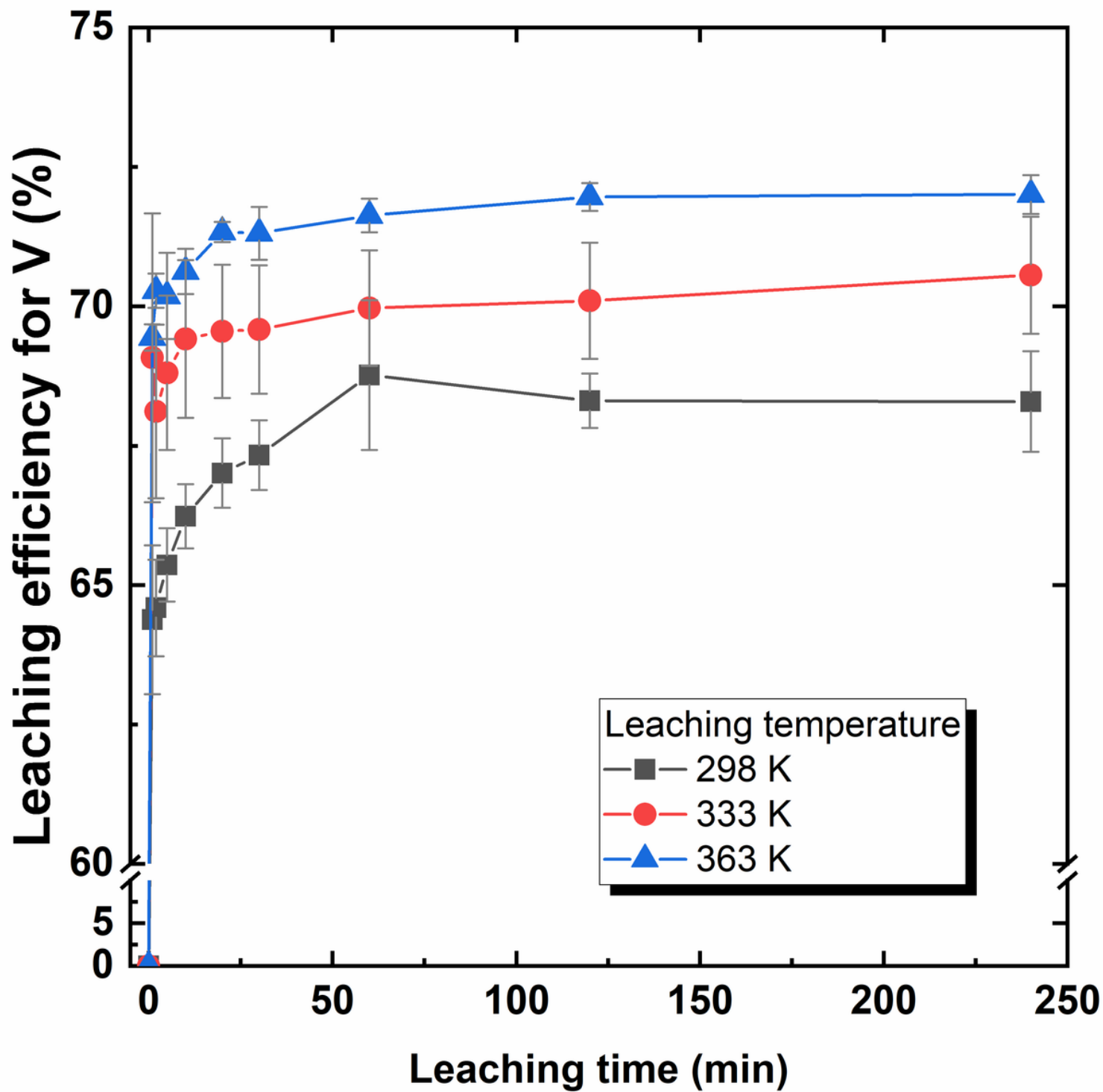


Figure 9

Effect of leaching temperature on the leaching rate of vanadium. The alkali-roasting was conducted at 1273 K for 2 h mixed with 30-wt% of Na₂CO₃.

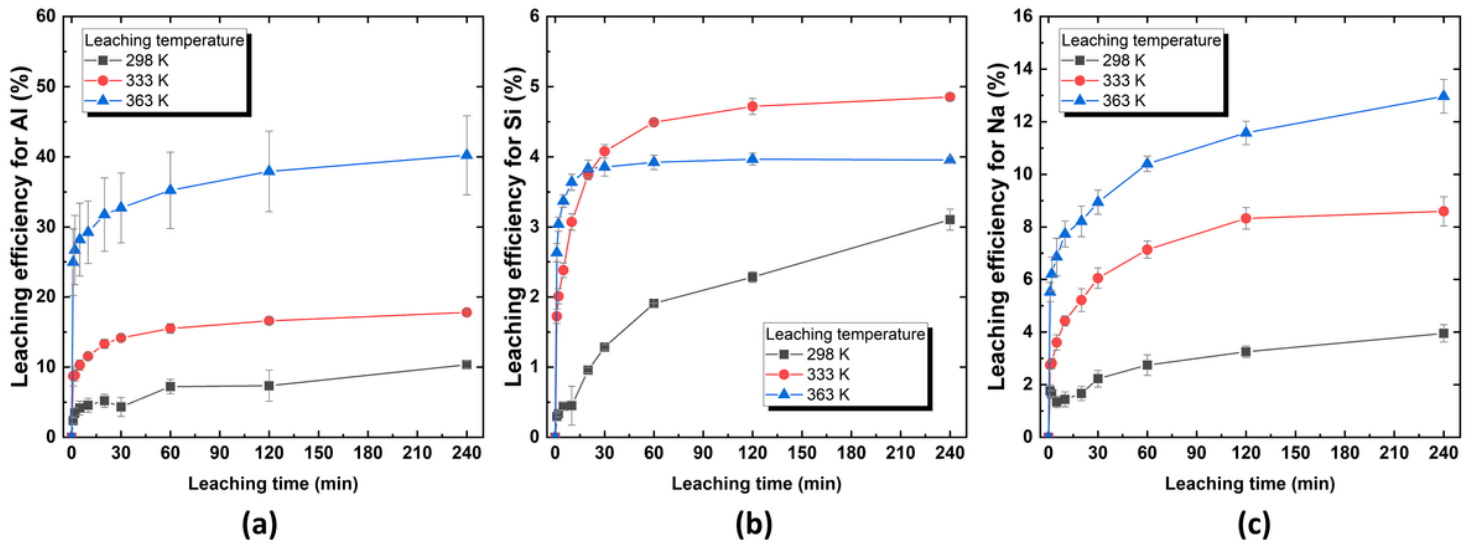


Figure 10

Effect of leaching temperature on leaching rate for (a) aluminum, (b) silicon, and (c) sodium. Alkali-roasting with 30-wt% Na_2CO_3 was conducted at 1273 K for 2 h.